Progress in Magnetic Sensor Technology for Sea Mine Detection

Ted R. Clem

Coastal Systems Station, Dahlgren Division, Naval Surface Warfare Center, Panama City, FL 32407

ABSTRACT

A superconducting magnetic-field gradiometer developed in the 1980's has been demonstrated in fusion with acoustic sensors to enhance shallow water sea mine detection and classification, especially for buried mine detection and the reduction of acoustic false alarm rates. This sensor incorporated niobium bulk and wire superconducting components cooled by liquid helium to a temperature of 4 degrees Kelvin (K). An advanced superconducting gradiometer prototype is being developed to increase sensitivity and detection range. This sensor features all thin film niobium superconducting components (replacing the bulk superconducting components used in the preceding generation) and a new liquid helium cooling concept. In the late 1980's, a new class of "high Tc" superconductors was discovered with critical temperatures above the boiling point of liquid nitrogen (77K). The use of liquid nitrogen refrigeration offers new opportunities for this sensor technology, providing significant reduction in the size of sensor packages and in the requirements for cryogenic support and logistics. As a result of this breakthrough, a high Tc sensor concept using liquid nitrogen refrigeration has been developed for mine reconnaissance applications and a test article of that concept is being fabricated and evaluated. In addition to these developments in sensor technology, new signal processing approaches and recent experimental results have been obtained to demonstrate an enhanced D/C capability. In this paper, these recent advances in sensor development and new results for an enhanced D/C capability will be reviewed and a current perspective on the role of magnetic sensors for mine detection and classification will be addressed.

Keywords: magnetic anomaly detection, magnetic gradiometer, superconductivity, Superconducting Quantum Interference Device, mine reconnaissance and hunting, unexploded ordnance detection

1. INTRODUCTION

Magnetic sensors have proven merit for mobile area surveys and search operations conducted from air, land or sea including application for the detection, classification, and localization of sea mines, unexploded ordnance (UXO), and chemical, biological and nuclear waste.[1-4] In fact, in an assessment conducted by the Jet Propulsion Laboratory for the

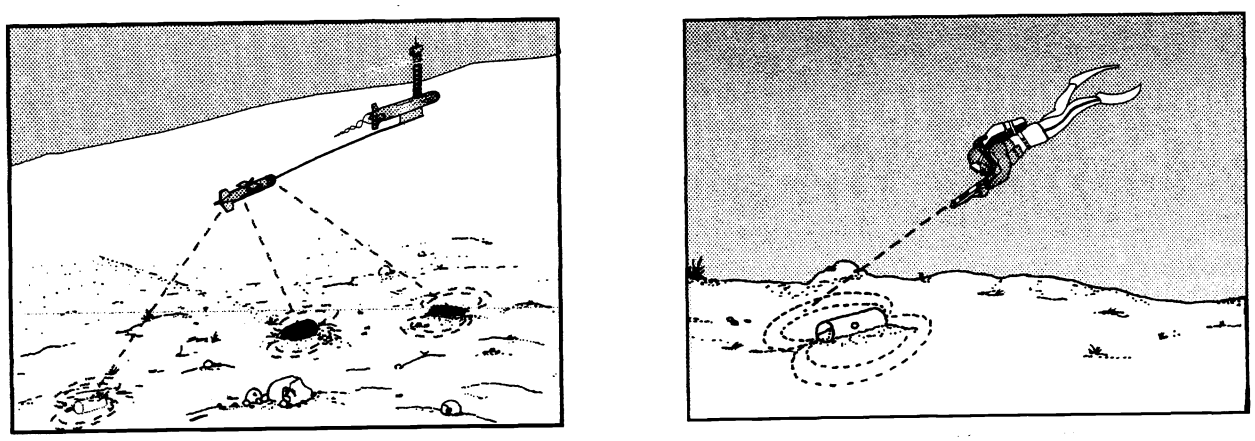

(a) (b)

Figure 1. Operationals scenarios for the magnetic detection and classifciation in sea mine countermeasures: (a) operation onboard an unmanned underwater towed vehicle towed behind a semi-submersible remotely-operated vehicle for reconnaissance and hunting and (b) diver-portable operation for diver mine detection and mine avoidance.

SPIE Vol. 3079 • 0277-786X/97/$10.00

Army Corps of Engineers, magnetic sensors in general were identified among the most useful sensors for UXO detection and localization, and superconducting gradiometers were specifically identified as the most useful tool in a class by themselves.[5] For applications in sea mine countermeasures, we can envision operational scenarios in which long-range detection is required for reconnaissance and hunting in preparation for an amphibious assault or shorter-range detection is required for diver mine detection and avoidance (Fig. 1).

In Sections 1.1 and 1.2, we shall describe two types of sensors which detect magnetic anomalies: sensors which detect changes in the local magnetic field, *magnetometers*; and sensors which measure the spatial derivatives of magnetic field, *(first order) gradiometers.*

Section 1.1. Magnetometers

The performance of a magnetic sensor is measured by its detection range, which is a function of its configuration and sensitivity and the magnetic moments of the targets of interest. In the far field, a target can be well approximated as a magnetic dipole. In this approximation, relatively simple, analytic expressions can be written to relate sensitivity requirements in terms of nominal values for target magnetic moment and range.

For the special case in which a circular, connected conducting loop with area A is carrying an electrical current I, we can define the magnetic moment of the loop as the vector $\mathbf{m} = IA\hat{\mathbf{n}}$ where $\hat{\mathbf{n}}$ is the normal to the loop in the direction defined by the right-hand rule for positive current. The International System (SI) unit for magnetic moment is ampere-meter-squared ($A\text{-}m^2$). The magnetic induction for a magnetic dipole can be written as

$$\mathbf{B} = \frac{\mu_o}{4\pi}\left[\frac{3(\mathbf{m}\cdot\mathbf{r})\mathbf{r}}{r^5} - \frac{\mathbf{m}}{r^3}\right] \tag{1}$$

The concept of magnetic moment **m** can be generalized for an arbitrary magnetic body and the magnetic induction of the body will approach the result of (1) in the far field. In air, the magnetic induction **B** is related to the magnetic field **H** via $\mathbf{B} = \mu_0\mathbf{H}$. Hereafter, **B** will be used exclusively and will be referred to as the magnetic field. The following units for magnetic field will frequently be used to represent sensor sensitivities: nanotesla (1 nT $=10^{-9}$ T), picotesla (1 pT$=10^{-12}$ T), and femtotesla (1 fT$=10^{-15}$ T).

A number of sensors, notably fluxgate magnetometers and superconducting magnetometers, measure the individual vector components of field. A three-axis vector magnetometer, likely using fluxgate or superconducting sensors, is very useful for localization (providing three channels of information). For stationary applications in geophysics and barrier defense, such sensors are effective. However, to date, these sensor types have not proven effective for mobile applications, since means to compensate the anomalous signals arising from rotations in the Earth's magnetic field have not been devised.

Other magnetometers, notably those based on nuclear or atomic resonance processes, measure the magnitude of the total magnetic field and are known as total-field magnetometers. Let $\mathbf{B}_0$ denote the magnetic field of the Earth, and let **b** denote the induction generated by an anomaly. If $|\mathbf{b}| << |\mathbf{B}_0|$, then the signal observed by a total field sensor (referenced to the baseline Earth field) is

$$b_m \equiv |\mathbf{B}_o + \mathbf{b}| - |\mathbf{B}_o| = \sqrt{B_o^2 + 2\mathbf{B}_o\cdot\mathbf{b} + b^2} - B_o \approx \frac{\mathbf{B}_o\cdot\mathbf{b}}{B_o} \tag{2}$$

As a result of the right-hand approximation above, a total-field magnetometer does not simply measure the magnitude of the magnetic-field anomaly, but measures instead the projection of that anomalous signal onto the earth's field.

Total-field magnetometers have provided the generally accepted method for magnetic anomaly detection. In particular, the AN/ASQ-81 and its successor the AN/ASQ-208 are total-field magnetometers utilized by the U.S. Navy for submarine detection from airborne platforms. A major advantage of this type of sensor is its insensitivity to rotation in the Earth's background field of 50,000 nT (since total field is a rotational invariant).

Measurements by total field magnetometers are difficult to interpret because these sensors effectively measure the projection of the anomalous magnetic field vector onto the Earth's magnetic field intead of the total field. Interpretation often requires an experienced operator, and precise anomaly locations are difficult to obtain. Since total field

The appearance of trade names in this document does not constitute endorsement by the Department of Defense, the Navy; or the Coastal Systems Station, Dahlgren Division, Naval Surface Warfare Center.

magnetometers provide only one channel of information, they lack valuable target vector information. In particular, they provide very limited localization and little capability for anomaly classification through moment determination. Moreover, these sensors are limited in field operation to sensitivities at levels approaching 0.1 nT as a result of geomagnetic noise, i.e., temporal variations in the Earth's field, without the use of very sophisticated compensation schemes.

Section 1.2. Gradiometers

The gradient of the magnetic field (in standard MKS units of T/m) is a second-order tensor with components given in Ref. 6 by

$$G_{ij} \equiv \frac{\partial B_i}{\partial x_j} = -\frac{3}{r^7}\frac{\mu_o}{4\pi}\{\mathbf{m}\cdot\mathbf{r}(r_i r_j - r^2\delta_{ij}) - r^2(r_i m_j + r_j m_i)\} \tag{3}$$

As a result of Maxwell's equations in free space, only 5 of these 9 tensor elements are independent. For this reason, (first order) gradiometers are typically designed with 5 independent gradient channels, using the minimum number which permits characterization of the local tensor gradient field.

It is feasible to determine the bearing vector and the magnetic-moment vector direction of the dipole by inversion of the gradient equations at a single point only.[6] More recently it has been shown that the addition of gradient rate information at a single point leads to a unique solution for dipole position and moment vector.[7]

The contraction of the gradient tensor defined by

$$G \equiv \sqrt{\sum_{i=1}^{3}\sum_{j=1}^{3} G_{ij}\,G_{ij}} \tag{4}$$

is a rotational invariant associated with the gradient tensor analogous to the magnitude of the field vector. This quantity may prove very useful for applications in which a gradiometer is subjected to large rotations during the period of measurement, e.g., hand-held operation (in contrast to straight runs onboard stabilized platforms).[6]

An example of one configuration to measure a single-gradient tensor component and a simple configuration to measure 5 independent gradient components are displayed in Figure 2. Each gradient tensor component is measured by a spatially separated loop pair connected in a common- mode rejection configuration. 3 vector magnetometers are included in the 5-channel gradiometer displayed in Figure 2(b) to compensate for the residual magnetometer signals in the gradiometer channels that arise as a result of manufacturing imperfections in the gradiometer loops.

Gradiometers offer the potential to remove many of the limitations associated with magnetometers because the output of a gradiometer is typically produced by twin magnetometers operating in differential mode. In particular, this configuration provides common-mode rejection of the nominal 0.1-nT temporal variations in the Earth's field and of the nominal 1000-nT field changes arising from typical 1 degree sensor rotations while in towed motion.

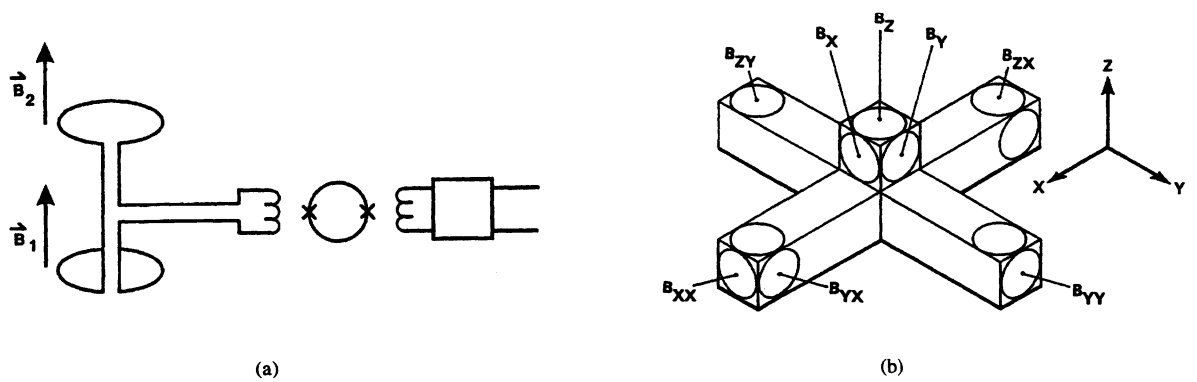

(a) (b)

Figure 2. Gradiometer sensor concepts including (a) a single SQUID-based gradiometer channel and (b) a conceptually simple 5-channel gradiometer configuration capable of magnetic dipole localization and moment classification (with 3 orthogonal magnetometers for motion compensation).

Gradiometers may be fabricated using many available magnetometer technologies. Available fluxgate and total-field magnetometers can perform at levels approaching 1-10 pT, while superconducting magnetometers utilizing Superconducting Quantum Interference Devices (SQUIDs) can perform at levels on the order of 1-10 fT. The extreme performance available from superconducting magnetometers provides a capability to fabricate gradiometers with high sensitivity having short baselines. The short baseline provides a compact package with extreme coherence between the magnetometers. The coherence is required to maintain high performance when in motion, and the compact package is amenable to implementation aboard one vehicle. In addition, with the compact sizes, a large number of gradient channels can be integrated into a small package to obtain complete position and moment determination of a magnetic dipole target at a single point in space.

Section 1.3. The Superconducting Gradiometer/Magnetometer Sensor

Almost all of the efforts with SQUID-sensor technology have dealt with sensors inside a very controlled laboratory environment, and to a more limited extent outside the laboratory at stationary locations, notably for geophysical measurements. During the 1980's, the Coastal Systems Station (CSS) developed the Superconducting Gradiometer/ Magnetometer Sensor (SGMS) specifically for mobile operations outside the laboratory environment (Fig. 3). The sensor employs largely niobium bulk and wire superconducting technology (with thin-film Josephson Junctions), features dc SQUIDs housed inside superconducting shields, and is convectively cooled to 4 degrees Kelvin by helium gas evaporating from a liquid helium reservoir. Under some field conditions, the SGMS has attained sensitivities on the order of 1pT/m-$Hz^{1/2}$ at 0.1 Hz. In comparison total-field gradiometers (with a 0.3-meter baseline) specifically designed for operation onboard a moving platform have achieved sensitivities on the order of 30 pT/m-$Hz^{1/2}$ at 0.1 Hz and a fluxgate gradiometer described in Section VII.A has achieved a sensitivity on the order of 300 pT/m-$Hz^{1/2}$ at 0.1 Hz.[1,2]

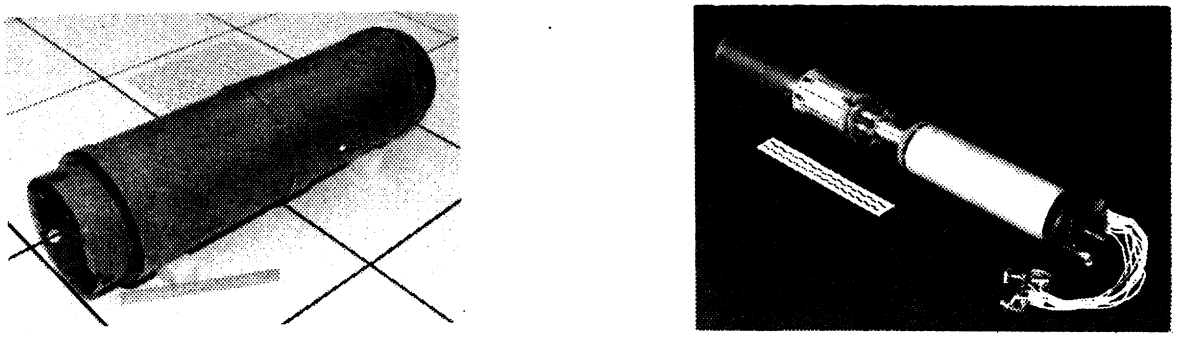

(a) (b)

Figure 3. Major subassemblies in the SGMS package: (a) dewar and (b) sensor probe unit.

The CSS initiated the Magnetic and Acoustic Detection of Mines (MADOM) Project starting in 1985. This project successfully demonstrated the value of magnetic and acoustic sensor fusion for mine reconnaissance and hunting. The SGMS demonstrated, for the first time, high sensitivity and rugged, robust, and reliable performance of a superconducting gradiometer operating outside the laboratory environment onboard a towed underwater vehicle with sea testing conducted for a period of 7 years. Gradiometer operation was automated (with the exception of semi-atuomated initial tuning) and fully-automated, real-time magnetic detection and classification signal processing was demonstrated to provide effective and accurate moment determination and localization for single and multi-target cases.[1,2]

Section 1.4. Quantitative comparison of magnetometers and gradiometers

The signal strength of a magnetic dipole decreases as the third power of the range for magnetic fields and as the fourth power of the range for magnetic field gradients. The approximate ranges of magnetometers and gradiometers are displayed in Figure 4 as functions of dipole strength and sensor sensitivity. It can be shown that the sensitivity requirements for a magnetometer and a gradiometer, respectively, to have the same detection range r against a given dipole target, is given by the approximate relation $N_g/N_m \sim 3/r$. For example, the detection of a mortar shell with a magnetic moment of 0.1 A-m^2 at

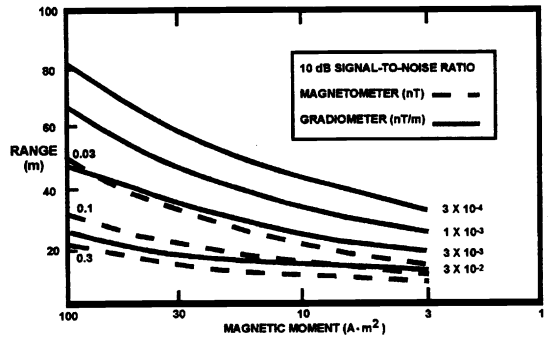

Figure 4. Approximate ranges (in meters) of magnetometers and gradiometers as a function of target strength in terms of magnetic moment (in units of A-m^2). Curves are given for different sensor sensitivities (in units of nT for magnetometers and nT/m for gradiometers assuming a 10-dB signal-to-noise ratio in both cases).

a range of 3 m, requires a magnetometer with sensitivity of 0.36 nT or a gradiometer with sensitivity of 0.36 nT/m (given a 10-dB signal-to-noise ratio for both cases).

It should be noted that the high rate of signal reduction with the fourth power of distance in the case of a gradiometer represents an apparent shortcoming for a gradiometer configuration. We believe that the ability to develop gradiometers with sensitivity greater than $1x10^{-3}$ nT/m for mobile operations and the extreme difficulty in utilizing magnetometers with sensitivity greater than 0.1 nT in mobile operations significantly outweighs this shortcoming. Moreover, the fourth power reduction of detection range with moment for a gradiometer has merit for the detection of targets with relatively small moments. For example, a 3 pT/m gradiometer can detect an individual 500-pound bomb (with a moment of 30 A-m^2) at a range of 33 m and a 60-mm mortar shell (with a moment of 0.1 A-m^2) at a range of 8 m. Hence there is only a factor of approximately 4 reduction in detection range for a 60-mm mortar shell compared to the 500-pound bomb although there is a factor of 300 in reduction of magnetic moment.

An example of the ease of interpretation for 5-channel gradiometer data compared to single-channel total-field magnetometer data is displayed in Figure 5. Magnetic profiles have been generated for a 60-mm mortar shell buried 1 meter under ground for two different orientations with respect to the Earth's background field. In this example, the magnetometer profiles and gradiometer profiles are given by the anomalous total field, Eq. (2), and the corresponding changes in magnitude of the gradient tensor, Eq. (4), respectively. The complex total field profiles require precision data and critical interpretation to localize dipole sources. The symmetric gradiometer profile leads to straightforward interpretation convenient for gradient searches for dipole localization.

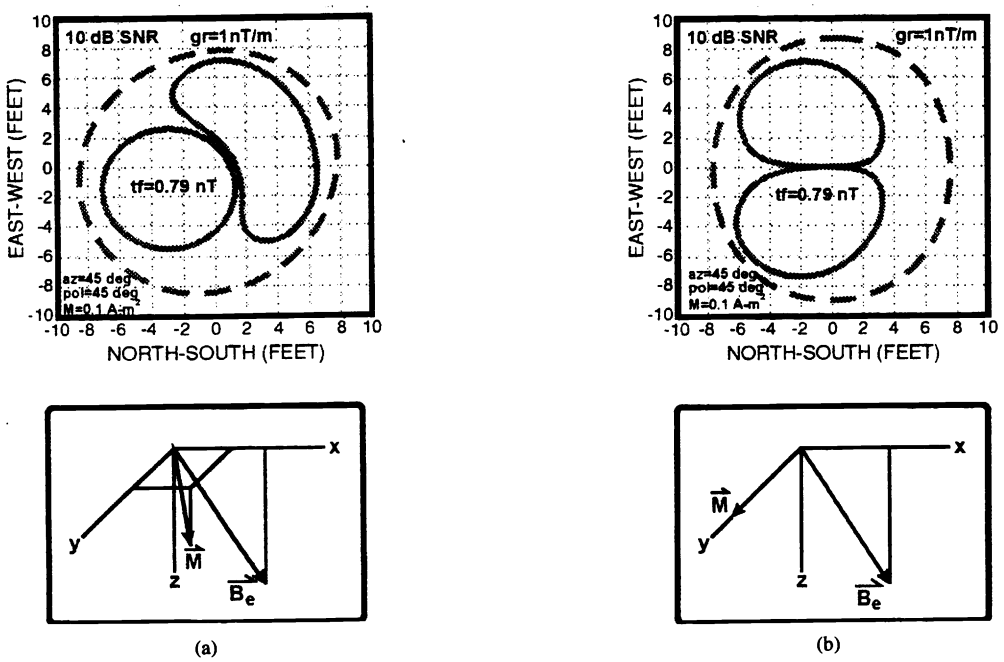

Figure 5. A comparison of magnetometer and gradiometer capabilities for target localization. The profiles measure tf = total field (Equation (2)) and gr = gradient magnitude (Equation (4)). Profiles are given for a magnetic dipole centered at origin with (a) a general orientation and (b) orientation in an east-west direction. Observe that the gradiometer profiles are approximately circularly symmetric about the dipole's location so that "gradient" searches normal to the gradient magnitude profiles are meaningful for the gradiometer. In contrast, the magnetometer profiles are not amenable to such straightforward interpretation.

2. SCENARIOS FOR GRADIOMETER MOBILE OPERATION

We can envision three general types of operational scenarios: relatively long-range rapid surveys for target clusters, more moderate-range searches against individual targets, and detailed close-in surveys. The selection of magnetic sensor type will largely depend on these operational requirements, determined primarily by the desired detection range, which is, in turn, a function of the magnetic moment of the targets and of sensor sensitivity. The selection also depends on such factors as financial budgets, logistical support and technical expertise of the operators. To date, magnetic sensor approaches have provided limited localization and mapping capabilities. To gain widespread acceptance, approaches must be introduced which provide accurate localization and target classification, and which lend themselves to straightforward interpretation and minimal training. Performance must not be limited by magnetic noise from the host platform and other subsystems. For land-based operations, the system must be capable of operating over rough, overgrown terrain. The sensor and associated signal processing also must deal effectively with environmental noise.

Section 2.1. General considerations

Long-range rapid surveys conducted from an aircraft have been proposed for initial surveys to locate clusters of UXO targets [4]. The mine reconnaissance/hunting demonstration of MADOM represents an example of a moderate-range search. Land-based manual surveys or diver operations for mine detection or avoidance provide examples of close-in surveys. High sensitivity will be critical for the long-range and moderate-range scenarios, but such sensitivity will likely be sacrificed for the close-in surveys at ground level. In fact, local geologic noise limits a gradiometer's noise floor to levels on the order of 0.05 up to 10 nT/m-$Hz^{1/2}$ which may limit the use of high-sensitivity gradiometers such as the SGMS for some land-based operations.

A perspective on the role of higher sensitivity gradiometers used for wide-area searches and lower sensitivity gradiometers for close-in surveys can be obtained from the following example (Fig. 6). A 3 pT/m gradiometer can detect a grouping of twenty 500-pound bombs (clustered in a circle several meters in diameter) at a range of 46 meters. An area search rate of 1 km^2/hr can be obtained when the sensor's altitude is 15 meters moving at a forward speed of 15 km/hr. When deployed from the ground, a less sensitive 300 pT/m gradiometer would provide detection ranges of 10 meters and 3 meters for the detection of a 500-pound bomb and a 60-mm mortar shell, respectively.

Two fundamental approaches for operation of a 5-channel tensor gradiometer stand out. First it will often be convenient to conduct straight-line searches at constant velocity for airborne and underwater vehicle operation and also for some

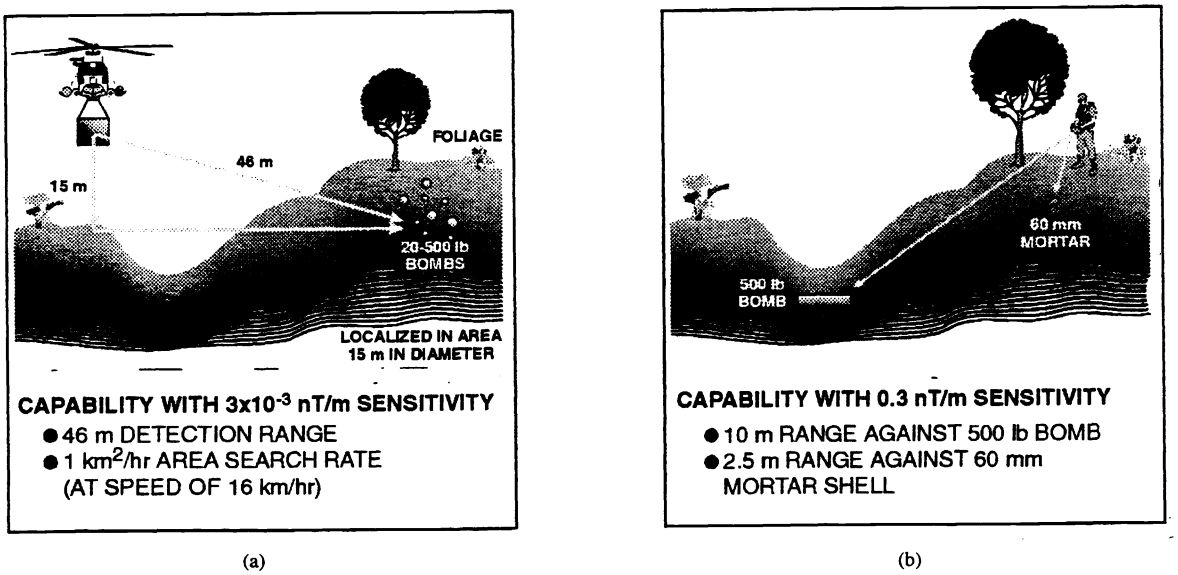

(a) (b)

Figure 6. Two modes of operation for 5-gradient channel sensors: (a) wide-area surveys using high sensitivity sensors and (b) short-range searches for single targets using less sensitive sensors.

land-based surveys if the terrain admits straight-line trajectories. For other cases, including many man-portable land-based and diver operations, it will be unreasonable to expect controlled operator motions along straight-line trajectories at constant velocities. In either case, we can implement signal processing using point-by-point inversion of the motion-compensated gradiometer signals. For the special case of straight-line searches, we can also utilize least-squares fit to the time series in order to improve target detection. One approach using point-by-point inversion is described in Section 2.2 and one approach using a least-squares fit is described in Section 2.3 below.

Section 2.2. Localization using point-by-point signal inversion

As mentioned above, the five independent gradient tensor components at a single point can be used to construct the bearing vector to a dipole source, and a scaled moment vector with the same direction as the dipole moment vector and a magnitude given by m/r^4.[6] The difficulty with this inversion is that there are multiple solutions: two nontrivially related solutions in a given half space, and two additional solutions obtained by reflection of the first two through an origin centered on the gradiometer. This multiplicity of solutions has limited the practical application of this algorithm. More recently, Wynn has investigated the use of the rate of change of the gradient tensor components, and their role in resolving the scaling and uniqueness issues associated with the gradient tensor inversion.[7]

For a sensor with specified translational velocity **v**, the time rate of change of the gradient tensor components has the form

$$\dot{G}_{ij} = \frac{3\mu_0}{4\pi r^9}\{35(\mathbf{m}\bullet\mathbf{r})(\mathbf{v}\bullet r)r_i r_j - 5r^2[(\mathbf{m}\bullet\mathbf{v})r_i r_j + (\mathbf{m}\bullet\mathbf{r})(v_i r_j + v_j r_i) + (\mathbf{v}\bullet\mathbf{r})(m_i r_j + m_j r_i) + (\mathbf{m}\bullet\mathbf{r})(\mathbf{v}\bullet\mathbf{r})\delta_{ij}] + r^4[m_i v_j + m_j v_i + (\mathbf{m}\bullet\mathbf{v})\delta_{ij}]\} \quad (5)$$

These equations have been inverted to give multiple solutions for the bearing vector and a scaled moment vector in the direction of the dipole moment vector with a magnitude given by m/r^5. The solution for bearing vector and moment vector direction common to the two inversions is unique, and the different scaling for the scaled moments in the two inversions yields the range to the dipole, resulting in a unique solution for **m** and **r** on a point-by-point basis. In practice, it is not necessary to specify a sensor velocity. All that is needed is knowledge of the position of the gradiometer relative to the Earth's reference frame. Work is ongoing to apply these algorithms to the practical interactive localization of buried UXO by means of a man-portable tensor gradiometer.

Section 2.3. Localization using a least-squares fit

A mathematical model for detection, classification, and localization (D/C/L) of multiple stationary magnetic dipole targets using a gradiometer (with 5 independent tensor gradiometer channels appropriately selected and 3 orthogonal magnetometer channels) moving in a straight line trajectory past the targets at a constant speed has been developed and validated in the MADOM project. The 5 output signals $S_i(t)$ (i=1,2,....5) from the 5 independent gradiometer channels and the 3 magnetic field components $B_l(t)$ (l =1,2,3) are measured as a function of time as the sensor moves past the targets. The time derivatives of field $dB_l(t)/dt$ are calculated from the $B_l(t)$ for eddy-current compensation. The objective of this model is to extract the dipole signals $G_{ij}^{(k)}(t)$ (k=1,2,...,n) for the unknown number n of dipole targets and then to determine the magnetic moments and the positions of the n targets.

The model describes the signals S_i in the 5 gradiometer channels by the equations

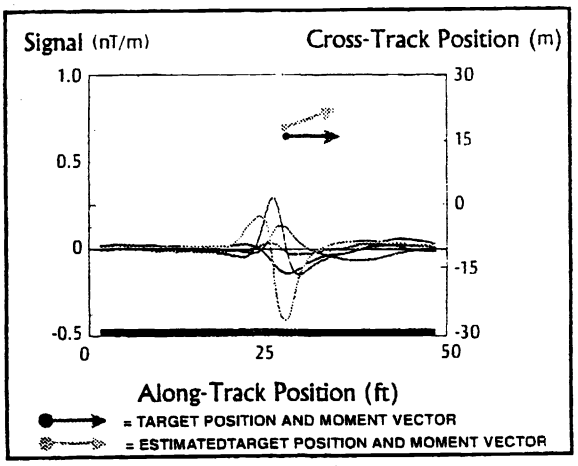

Figure 7. The five gradiometer signals in a 45-m section of data on a pass near a Mk83 1000-lb bomb.

$$S_i(t) = \sum_{j=1}^{5} c_{ij}\left\{\sum_{k=1}^{n} G_{ij}^{(k)}(t)\right\} + \alpha_i + \sum_{l=1}^{3} \beta_{il} B_l(t) + \sum_{l=1}^{3} \gamma_{il} \dot{B}_l(t) + \nu_i(t) \quad (6)$$

where c is the pre-determined calibration matrix for the gradiometer, $\nu_i(t)$ and α_i are uncompensated noise (setting the noise floor of the channel commpensation parameters per channel) and channel biases, respectively, and β_{il} and γ_{il} are the balance and eddy-current vectors for channel i. An iterative analysis first estimates the α's, β's and γ's (a total of 35 parameters) and then executes a gradient search for the location of the single target that best fits the residual signal. The α's, β's and γ's, and target location and moment are then optimized, and the procedure is repeated for a second target. Targets continue to be added until finally no target can be found whose signal contributes substantially to a reduction in total signal power, at which point the algorithm terminates.

Fig. 7 displays the motion-compensated signals obtained from the gradiometer and the information extracted from the algorithm in detecting a 1000-lb Mk83 bomb. The five gradiometer signals are displayed for a 45-m section of data with the bomb located 15 m to port and 5 m below the gradiometer at the closest point of approach. The measured and predicted target location, moment, and orientation are also displayed to indicate the capability of the algorithm to provide good fits to the data.

3. MOBILE UNDERWATER DEBRIS SURVEY SYSTEM

A project has been initiated to develop and evaluate a Mobile Underwater Debris Survey System (MUDSS) capable of finding and accurately mapping the locations of UXO ranging from small shells to large bombs in water depths of from 4 to approximately 100 feet in coastal regions at formally used defense sites.[3] The effort involves a collaboration between CSS and the Jet Propulsion Laboratory].[8] In addition to the application of UXO detection at coastal sites utilizing underwater towed sensor suites as described in this section, the use of a superconducting gradiometer in a system concept for rapid airborne reconnaissance and survey of UXO sites has been proposed.[4]

Section 3.1. General project description

The MUDSS project is divided into two phases. Phase I, which ran for one year and culminated in an at-sea feasibility demonstration of a multi-sensor MUDSS prototype against UXO in a drill target field. The feasibility demonstration was successfully executed in August and September of 1995 in St. Andrews Bay (near Panama City, FL) with the SGMS utilized for magnetic detection. Phase II will culminate in 1997 in a technology demonstration consisting of a UXO survey at a yet-to-be-determined formally used defense site.

Figure 8 depicts the first version of the MUDSS system which was fielded in 1995 for the feasibility demonstration. The surface craft is a custom designed, magnetically and acoustically quiet, shallow draft, trailerable catamaran. A dead-weight

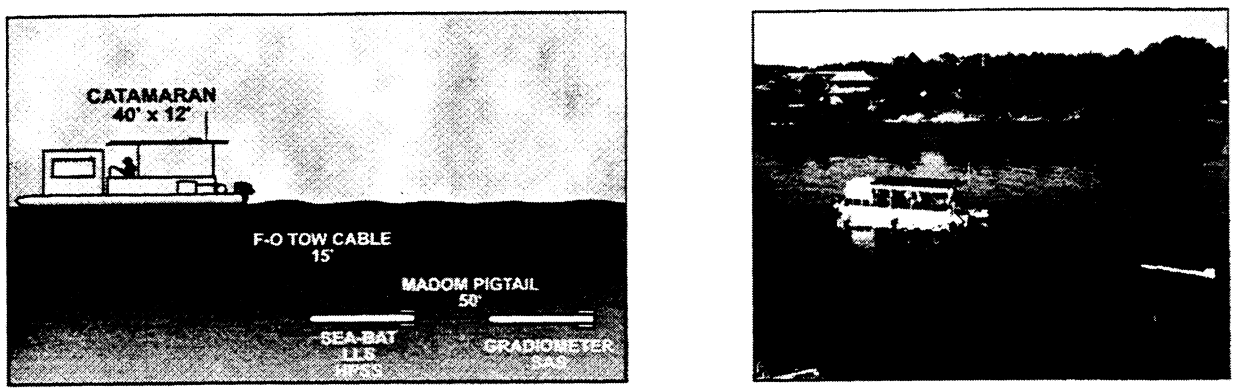

(a) (b)

Figure 8. The Mobile Underwater Debris Survey System: (a) artist's concept detailing key features of the system and (b) photograph of system in transient to test site with the dead-weight depressor housed out of water for speed and maneuverability.

depressor is suspended off of the back of the catamaran to maintain the appropriate depth for sensor operation and to house part of the sensor suite (a RESON Seabat ahead looking sonar, a CSS-developed high frequency sidescan sonar, and a Raytheon-leased LS 4096 laser linescanning electro-optic sensor. A second neutrally buoyant tow body trailing the deadweight depressor houses a CSS-developed low frequency synthetic aperture sonar and the SGMS. Reference 3 gives a detailed description of the feasibility demonstration test field layout, the testing procedures, and the performance of the acoustic and electro-optic sensors. Specific details relevant to the gradiometer demonstration are given here.

Section 3.2. Gradiometer results from the Feasibility Demonstration

A linear target field was laid out to evaluate the SGMS performance. The field consisted of a row 200 m in length of eight small and medium-sized targets (mortar and artillery shells ranging in caliber from 60 up to 203 mm) running north-south; a second, shorter row of three medium-sized targets (two oil drums and a Mk82 500-lb bomb) parallel to, and 9 m east of, the first row; and a third row of two targets (a Mk83 1000-lb bomb and a Mk84 2000-lb bomb) 9 m east of the second row. A marker and a sonar calibration panel with ferrous anchors were laid at one end of the linear field. Estimates of the magnetic moments for the targets obtained from the D/C/L algorithm described in Section 2.3 are tabulated in Table 1. These magnetic moments ranged from 0.03 A-m^2 for one 60mm mortar shell up to 120 A-m^2 for the 2000-lb bomb.

TABLE 1

ESTIMATES OF MAGNETIC MOMENT FOR THE UXO TARGETS

Target	Moment (A-m^2)	Range (m)	Relative Range
60mm shell	0.03 - 0.2	6 - 9	1-1.5
81mm shell	0.3	10	1.6
105mm shell	0.7	13	2.2
175mm shell	3	18	3
203mm shell	5	22	3.6
55 gal oil drum	10 - 25	27 - 32	4.5 - 5.3
500-lb bomb	20	30	5
1000-lb bomb	40	36	6
2000- lb bomb	120	48	8

The detection range for these targets is also tabulated in Table I. Absolute range is given for a gradiometer with sensitivity of 3 pT/m-Hz$^{1/2}$ at 0.1 Hz assuming a 10 dB signal-to-noise ratio and relative range is given for fixed gradient sensitivity (normalized to 1 for a 60mm shell with magnetic moment of 0.03 A-m^2). Observe that the 2000-lb bomb is detectable at 8 times the range of the 60mm mortar shell.

The predicted results from the D/C/L algorithm to estimate location and to classify the targets according to magnetic moment are displayed in Fig. 9 for one pass of the system through the target field. Open circles designate the actual location of the targets, while the solid circles indicate the predicted positions. The size of the solid circles indicate the magnitude of the targets' magnetic moment. For the feasibility demonstration, the nominal performance of the gradiometer channels was on the order of 3 pT/m-Hz$^{1/2}$ at 0.1 Hz. The D/C/L algorithm was effective in localization and classification (by moment magnitude) all of the targets in this pass with the exception of the 1000-lb Mk83 bomb. This exception provides an example of multi-target localization for which there are 2 targets (the 500-lb bomb and the105mm shell) in this data window in addition to the 1000-lb bomb. In this case, the algorithm successfully localized the 500-lb bomb and the 105mm shell with high signal strength, but failed to locate the more distant 1000-lb bomb with a relatively weak signal strength. The ferrous anchors for the marker and calibration panel at the right hand side of the map and two clutter objects in proximity to the 106mm shell (not a part of the target set) were also detected during this run. Double detections are displayed in Figure 9 for two targets, the 500-lb bomb and one of the two oil drums. These represent target detections by

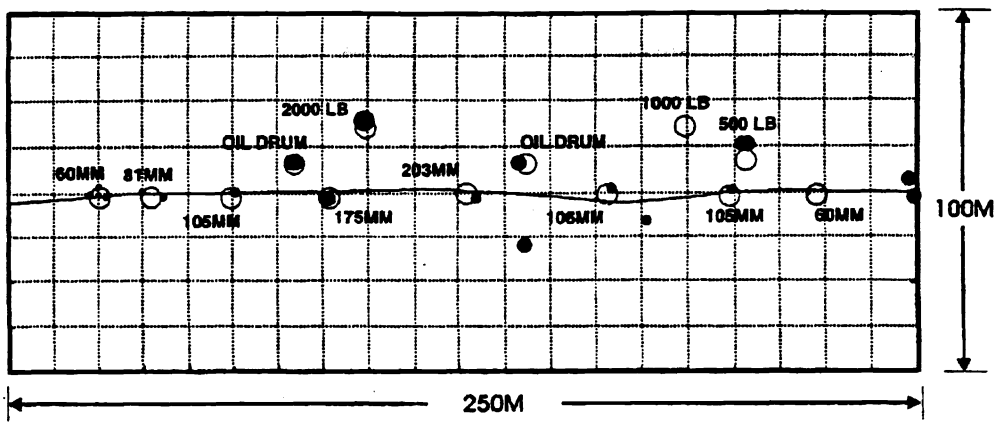

Figure 9. Gradiometer targets found in one run over the linear field with the open circles ○ indicating the actual target locations and the solid circles • indicating the positions predicted by the D/C/L algorithm. The size of the solid circles • indicates the predicted magnitude of the target's magnetic moment.

the D/C/L algorithm in two separate data segments. The high degree of overlap for the double detections is suggestive of the degree of accurarcy obtained with this algorithm.

4. CLUTTER REJECTION

Generally active acoustic approaches have proven to be an effective means to detect, classify and localize tethered sea mines or bottom mines proud with respect to the bottom in deeper waters. However the shallow-water bottom mine environment is an especially difficult acoustic environment in which to operate. Interfering reverberations from the air/sea and sea/bottom interfaces, bottom topographical features, general harbor debris, and mine burial present a difficult acoustic environment for bottom mine detection. In coastal regions, the density of debris clutter may lead to a high false-alarm rate using conventional imaging sonar approaches alone.

For effective clutter rejection, it is very desirable to use distinctly different sensor approaches. The application of two or more collocated sensors operating simultaneously has the potential to reduce false alarms and provide robust detection in a wide variety of background conditions. For mine reconnaissance and hunting, the combination of magnetic sensors with sonars provides such an alternative. In the MADOM sea testing, more than 90% of the acoustically mine-like clutter was not magnetically mine-like.

Several investigations have been conducted recently using automated neural network approaches to assess the merit of magnetic and acoustic data fusion.[9,10] The following result was obtained courtesy of L. Smedley and G. Dobeck.[10] A set, consisting of 215 sonar images containing an assortment of drill targets and clutter objects, was assemblied using data collected from sea tests with the SGMS and the MADOM low frequency synthetic aperature sonar. For each sonar image, the magnetic detections were co-registered. An attractor-based k-nearest neighbor neural network was developed using the magnetic and acoustic features given in Table 2.

TABLE 2

FEATURES USED TO TRAIN THE NEURAL NETWORK DEVELOPED IN [10]

Magnetic Features	Acoustic Features
Total magnetic moment	Average signal-to-noise ratio (SNR) over object's length
Y-component of moment	Average SNR over object's width
Z-component of moment	Maximum of the ratio of SNR for length to SNR for width
Depth estimate	Number of intense pixels
Confidence level for correct object classification and localization	Target length
	Target width
	Estimated clutter density

Receiver operating curves (ROCs) for this data were established for different detection ranges, recognizing the fact that the two sensors are effective over different ranges. The ROC for the individual sensors and for the two-sensor data fusion (obtained from this neural network) are displayed in Fig. 10 for tracks on both sides of the vehicle in a range where both sensors were effective. For these tracks, there were 93 drill targets in the 215 images.

We observe in this figure the improved detection and classifcation obtained using the data fusion. For an acceptable rate of 0.1 false alarms per image, the probability of detection and classification was 0.5 for the acoustic sensor alone and 0.77 for the magnetic sensor alone. The probability of detection and classification increased to 0.9 for a rate of 0.1 false alarms per image using this neural-network data fusion. Although these results were taken from a small data set of 215 images, we believe that the trend clearly demonstrates the substantial benefit of magnetic and acoustic data fusion for shallow water mine reconnaissance and UXO survey.

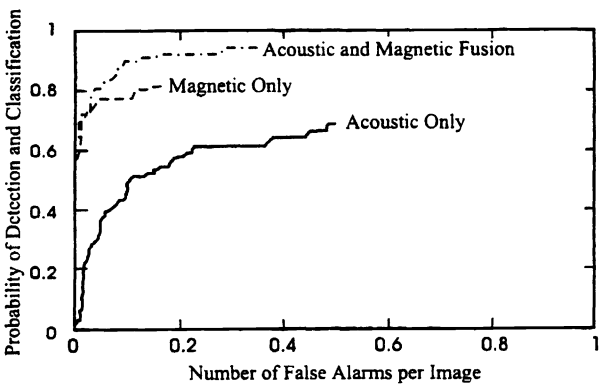

Figure 10. The probability of detection and classification for acoustic and magnetic sensors alone and for neural-network fusion data from both sensors given as a function of the number of false alarms per image in the two tracks from 10 to 27 meters on either side of the vehicle.

5. THE THIN-FILM GRADIOMETER

We believe that the current technology, represented by the SGMS sensor, is reaching its performance limit. This technology is largely characterized by the use of bulk and wire niobium (Nb) superconducting components. Advances in Nb thin film technology to obtain increased low frequency sensitivity and the relative simplicity of the thin-film processing in contrast to labor-intensive assembly of bulk SQUID packages and the hand winding of wire loops are appealing. For mobile applications, the greater intrinsic balance, i.e., common-mode rejection of the Earth's magnetic field, obtained from thin-film lithography compared to manual winding of wire loops and the removal of bulk magnetic components, including superconducting diamagnetic components such as shield canisters, is important to reduce anomalous signals in the gradiometer sense loops arising from acceleration-induced relative motion of parts. A project to develop a high sensitivity, all thin-film gradiometer sensor for mobile deployment is being pursued by the CSS, IBM Research[11], Ball Aerospace[12],

Lockheed-Martin[13], Quantum Magnetics[14], and the Naval Research Laboratory[15] for mine reconnaissance and UXO survey demonstrations.

Section 5.1. Cryogenic and room-temperature electronics

Major advances in Nb thin-film fabrication technology has led to the development, for the first time, of high quality low frequency SQUID-based magnetic sensors utilizing Nb-AlO_x-Nb tri-layer technology on a 5" scale. This work has led to the production of totally unshielded gradiometers which have been successfully demonstrated to operate in the Earth's magnetic field.

A cryogenic probe assembly for high performance in mobile operation has been manufactured with 3 tensor gradiometer circuits mounted on a single-crystal silicon rod and mounted to the dewar neck plug (Fig. 11). The gradiometer circuits consist of 2 counterwound magnetometer loops, each 3.8 cm square with a baseline of 5.3 cm, monolithically coupled to the SQUID. The precision lithography in conjunction with a configuration in which the sense loops, the SQUID washers, and their modulation and feedback coils are all patterned as gradiometers has provided extreme balance in order to maintain full sensitivity in the presence of field changes on the order of 1000 nT.

A benchtop version of high frequency flux-lock loop (FLL) feedback electronics with a modulation frequency of 16 MHz, a factor of 15 to 30 times the current frequency available with commercial electronics, has been developed in order to assure specified signal-to-noise ratios required from the all thin-film gradiometer channels (using air-core thin-film output transformers in place of wire-wound ferrous-core transformers) and to provide a high bandwidth for electromagnetic interference immunity.[16]

Section 5.2. The Advanced Liquid Helium Dewar

A dewar prototype, referred to as the Advanced Liquid Helium Dewar, was developed to assure that the dewar would not limit sensor performance (Fig. 12). A flexible design approach supported by detailed thermal, mechanical and field calculations was pursued. Stringent material selection and magnetic screening standards were established. The materials typically were chosen to be as magnetically clean as possible, with residual magnetizations 10 orders of magnitude smaller than that for soft steel. The magnetic gradient stability and the eddy current stability are 100 times better than the preceding state-of-the-art established with the SGMS.

An exchange gas cooling approach was pursued in place of the convective cooling utilized in the SGMS dewar. New innovations for thermal management have been implemented - anti-slosh baffles, thermal filters to isolate sensor area from bath temperature fluctuations, aluminized-mylar blankets for radiation shielding custom etched to reduce the eddy currents, and thermal networks of 99.999% pure aluminum wire for temperature uniformity. Temperature stability in motions typical of tow operations is on the order of 1 $\mu K/Hz^{1/2}$ at 0.1 Hz, a factor three orders of magnitude better than for the SGMS dewar.[17]

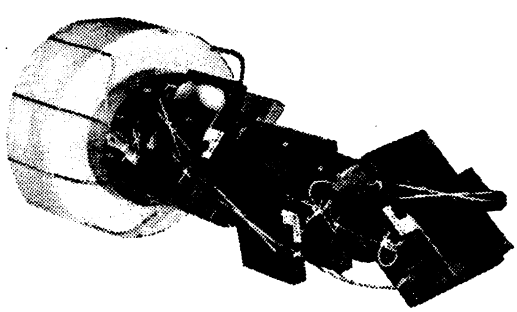

Figure 11. The TFG Cryogenic Probe Assembly.

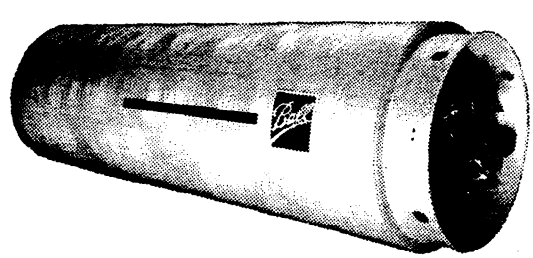

Figure 12. The Advanced Liquid Helium Dewar.

Section 5.3. Field testing of the integrated sensor

The integrated sensor prototype has been evaluated recently under field conditions. For this testing, the benchtop room temperature FLL electronics (which have a significant magnetic signature) are operated off a 15-m cable outside the test facility (remotely positioned some 13 m away from the sensor so as not to limit the performance of the sensor in motion). Stationary measurements have been conducted in this test setup in order to establish a baseline for the motion testing; i.e., to quantify any deterioration of performance in motion. In this configuration for the sensor, white noise on the order of 50 fT/m-Hz$^{1/2}$ (10 $\mu\Phi_0$/Hz$^{1/2}$) has been demonstrated. The knee for 1/f noise occurred at approximately 1 Hz and the noise floor rose to approximately 200 fT/m-Hz$^{1/2}$ (40 $\mu\Phi_0$/Hz$^{1/2}$) at 0.1 Hz. The nominal balance of the gradiometers is estimated at $1x10^{-4}$/m (as measured indirectly from a comparison of compensated and uncompensated motion spectra obtained in preliminary motion testing), a factor of at least 20 greater than obtained with the wire-wound SGMS loops without the trimming procedures required for wire loops. The dynamic range of the gradiometers is $6x10^6$.

For comparison, these electronics evaluated in a laboratory environment (integrated with a preliminary version of the gradiometer circuit currently being evaluated) operating off a 2-m cable has white noise on the order of 4 $\mu\Phi_0$/Hz$^{1/2}$ with about 1/3 of the noise from the preamplifier. The knee for 1/f noise also occurred at approximately 1 Hz and the noise floor rose to approximately 7 $\mu\Phi_0$/Hz$^{1/2}$ at 0.1 Hz. The electronics demonstrated a very high closed loop bandwidth exceeding 2.5 MHz and a very high slew rate greater than $1x10^6$ Φ_0/sec at frequencies up to 1 MHz.[16] In comparison, the SGMS has a bandwidth of 100 kHz and a slew rate of $2.5x10^4$ Φ_0/sec.

Section 5.4. Development of a field-deployable TFG

The existing TFG is being upgraded to a ruggedized field-deployable version. A fully-populated 5-channel cryogenic probe assembly is being developed to replace the 3-channel laboratory unit. A compact field-deployable room-temperature electronics package is being developed to replace the benchtop FLL electronics currently utilized for the laboratory version and to provide automated sensor control, signal digitization, and data linking. Miniaturization of the electronics into a single integrated unit mounted onto the sensor (as required to obtain sensitivity of the integrated sensor in motion) represents a major undertaking. The entire analog and digital electronics for 5 gradiometer and 3 magnetometer channels is being packaged into a unit 43 cm in diameter and 56 cm in length. The package must have magnetic signature consistent with the sensitivity requirements in motion, power reduced by a factor of 30 compared to the laboratory prototype, and dimensions to minimize the length of the sensor body section for underwater deployment as much as possible. Production is in progress with final assembly and testing to be completed in 1997 for integration in an underwater tow system for mine hunting and for UXO surveys.

6. HIGH Tc SUPERCONDUCTING TECHNOLOGY

As a result of nitrogen cooling, the development of sensors utilizing the high-T_c materials with nitrogen cooling provides an opportunity for significant size reduction, an ease of maintainability and convenience in comparison to the low-T_c technology with helium cooling, factors critical to gain widespread acceptance of the superconducting technology over other magnetic sensor approaches.

Section 6.1. Perspective on nitrogen cooling for naval operations

A broad-based assessment of refrigeration technology including liquid, solid, and triple-point nitrogen dewars and active cryocoolers was conducted.[1,18] The conclusion from this assessment is that liquid nitrogen dewars represent the best choice for near-term development of a high performance high T_c superconducting gradiometer for mobile applications. The design for an open (vented) liquid nitrogen dewar with dimensions 45 to 75 cm in length and 30 to 50 cm in diameter has been established consistent with sensitivity goals (Fig. 13). These dimensions are consistent with available space in underwater tow bodies of interest for U.S. Navy applications. A final choice for

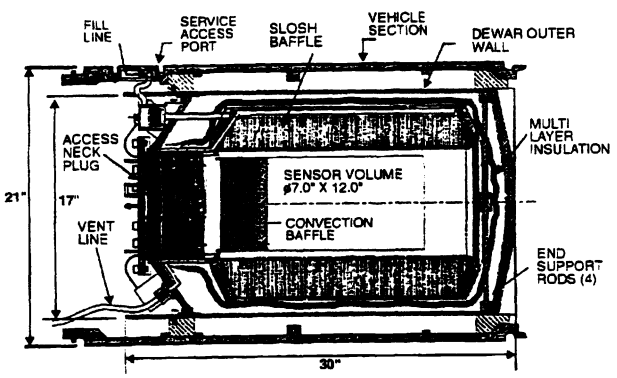

Fig. 13. Liquid nitrogen dewar concept with design versatile for multiple applications. This dewar has an outer diameter of 43 cm (17") (compatible with operation in a 53-cm (21") vehicle) and a length of 75 cm (30"). The dewar is projected to have a hold time of 33 days.

dimensions in any final dewar design would be based on a tradeoff between space and hold time. Results of the concept analysis indicate that a dewar with dimensions of 43 cm in diameter and 75 cm in length would have a hold time of approximately 33 days. This hold time is over 6 times greater than the hold time for the Advanced Liquid Helium Dewar which has the same diameter but is 150 cm long, twice the length of the nitrogen dewar.

The benefits for naval mobile applications which can be obtained from these reduced cryogen requirements include: (1) a significant reduction in down time during operations; (2) affiliated reductions or elimination in labor requirements for cryogen support during critical phases of an operation; (3) reduced failures in the cryogenic circuits or in the dewar (such failures typically occur during cryogen recycling); and (4) the elimination of an additional footprint on ship deck required for helium storage. In addition, the use of liquid nitrogen in place of liquid helium significantly reduces supply logistics as a result of the wide availability of nitrogen on the market at domestic and most foreign ports and the availability of a large number of liquifiers in the U.S. Fleet, with at least 54 units identified. Significant cost savings are expected from reduced costs for cryogen supply.

Section 6.2. Device development under this project

Since 1993, there have been a number of laboratory results reported on magnetometer prototypes with white noise better than 200 $fT/Hz^{1/2}$. A number of test samples, magnetometer circuits and gradiometer circuits have been developed in conjunction with this project. This included a report of 26 $fT/Hz^{1/2}$ at 1 Hz for a 2x2-cm magnetometer.[19] As an element of this program, the impact of flux trapping for unshielded operation of high T_c sensors in the Earth's magnetic field has been investigated and identified to be more problematic than for the corresponding low T_c niobium thin-film sensors. Approaches are being pursued to circumvent current limitations in high T_c fabrication technology.[20-24] In particular, the three-sensor gradiometer approach described in Section 7.2 is an example of one means to circumvent these limitations. In that approach, magnetic-field coils are utilized to null out the Earth's magnetic field at the sensing circuit. The field nulling significantly reduces noise associated with non-ideal magnetization effects in the high-T_c superconducting material.

Section 6.3. 3-Axis High Tc magnetometer

A 3-axis magnetometer prototype developed by Conductus under a SBIR contract has been evaluated (Fig. 14). This sensor is being developed for stationary operation with a focus on geophysical applications. Results obtained to date are very promising. The sensor has been operated in the field totally unshielded without any deteriorated performance compared to its performance shielded. Magnetometer performance of 140 $fT/Hz^{1/2}$ at 1 Hz has been demonstrated under stationary field conditions. This performance is a factor over 50 times better than the performance obtained from the best commercial fluxgate magnetometers. The 3 High-T_c SQUID magnetometer circuits in this unit have been working reliably for over one year without failure.[25]

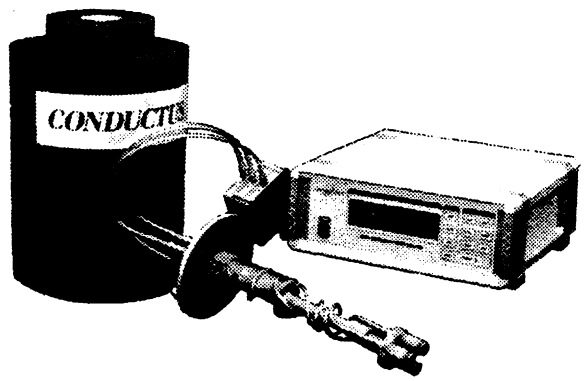

Figure 14. 3-channel high-T_c magnetometer.

7. THE THREE-SENSOR GRADIOMETER

One advantage of the niobium-based superconducting technology, especially for mobile operation, is the ability to fabricate large scale counter-wound gradiometer sense loops using either niobium wire or multi-layer thin films with crossovers. This allows signal subtraction using very low-noise passive circuits prior to signal processing with active amplifier circuits, which greatly reduces dynamic range requirements from the active electronics. A gradiometer can be configured using two independent magnetometers with signal subtraction performed at the output of the two magnetometers. The CSS pursued this approach in the early 1970's using fluxgate technology. Good stationary performance was obtained at that time, but there was insufficient dynamic range in the processing of the differential signals to operate the sensor in motion.

In order to circumvent this dynamic-range limitation arising by differencing two individual magnetometer signals during mobile operation, a novel approach patented by IBM Research is being pursued.[26,27] A third magnetometer is used for

common mode rejection, feeding back a signal to the two primary magnetometers which nulls out the ambient background field. This concept is denoted as the three-sensor gradiometer (TSG). The concept is depicted in Fig. 15 for one case in which there are two primary high T_c SQUID-based magnetometers and a third fluxgate magnetometer for field nulling.

Section 7.1. Fluxgate version of the TSG

The basic TSG concept has been successfully pursued using room temperature fluxgate magnetometers (in place of the SQUID magnetometers). A laboratory prototype of the fluxgate TSG has been developed and demonstrated (Fig. 16). This sensor features four commercial 3-axis triad sets of fluxgate magnetometers in a planar square array with a one-foot diagonal baseline. One triad set of fluxgate magnetometers serves as a reference to measure the 3 mean magnetic field vector components at the array. The remaining three sensor triads are each mounted inside their own 3-axis Helmholtz coil sets which null the mean magnetic field at the sensor triad. The residual signals at the triads are processed through their commercial electronics and appropriate combinations are subtracted via differential amplifiers. In this manner, 6 tensor gradient terms can be calculated of which 5 are independent. In the laboratory prototype, analog electronics are utilized to implement the magnetic feedback currents with manual feedback adjustments determined to an accuracy of 5 decimals by a digital signal-processing routine. Sensitivity better than 0.3 nT/m at 0.1 Hz in motion has been demonstrated.[28,29]

A Phase I SBIR has recently been awarded to Quantum Magnetics to develop a ruggedized field-deployable version designed to improve the performance of the laboratory prototype. This version will be compact and light weight for man-portable operation. It will feature an integrated computer for fully automated sensor control and signal processing and a display to provide the operator easy target detection, classification, and localization.

This sensor offers the opportunity to become the mainstay for man-portable magnetic surveys, replacing the total field magnetometer by offering unambiguous detection, moment classifcation, and localization. Although its range will be limited by factors of 4 to 10 compared to the superconducting gradiometers described previously, this type of sensor will provide a low cost approach convenient for many applications and will avoid a need for cryogens.

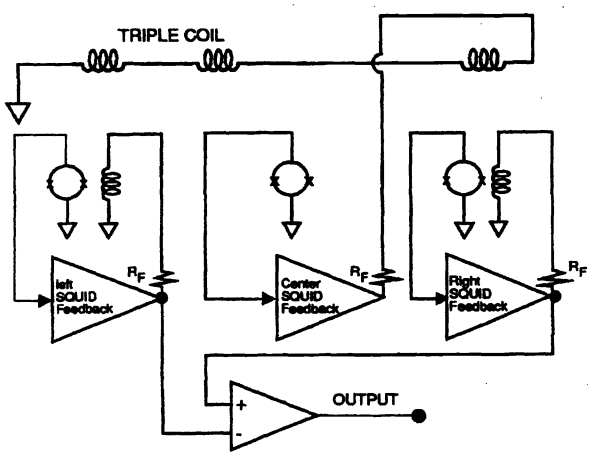

Figure 15. The three-sensor gradiometer concept for one case in which there are two primary high T_c SQUID-based magnetometers and a third fluxgate magnetometer for field nulling.

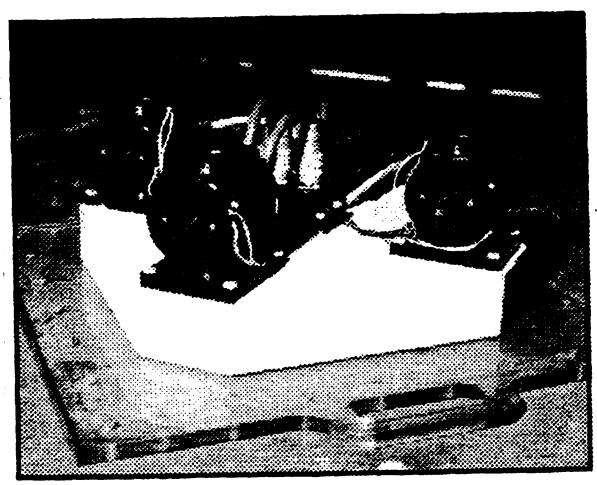

Figure 16. Laboratory prototype of a 5-channel fluxgate gradiometer utilizing the three-sensor -gradiometer concept.

Section 7.2. High Tc version of the TSG

A project to develop and to demonstrate feasibility of a compact field-deployable high-T_c superconducting gradiometer concept for mobile operation is being pursued by the CSS, IBM Research, Ball Aerospace, Quantum Magnetics, the Naval Research Laboratory, and Lockheed-Martin. As mentioned previously, it has been possible to fabricate high-sensitivity gradiometers in niobium technology by using monolithic wire or thin-film counterwound sense loops. Neither wire or

thin-film monolithic loops can currently be manufactured using the high-T_c technology to provide the higher sensitivities in motion offered by niobium technology. A high-T_c gradiometer preliminary design has been established based on the TSG concept and its performance in motion has been modelled. The TSG approach circumvents the current limitations in high T_c manufacturing technology, providing long baselines by using normal metal wire to connect the two SQUID magnetometers. Further improvement in performance is expected using the high T_c SQUID magnetometers in place of fluxgate magnetometers as a result of their intrinsically greater sensitivity. A laboratory test article is being developed to evaluate this concept (Fig. 17). This test article incorporates two flux cubes with each flux cube consisting of 3 orthogonal high-T_c SQUID-based magnetometers with dimensions of 1 cm^2. The two cubes, separated by a baseline of approximately 30 cm, permit the synthesis of 3 tensor gradient components. For this test article, a 3-axis fluxgate triad is used to provide the 3 reference channels required in the feedback loop to null out the mean ambient background field. This high T_c gradiometer is expected to surpass significantly the motion performance of any conventional non-superconducting magnetic sensor technology and is projected to have sensitivity better than that of the low-Tc SGMS.

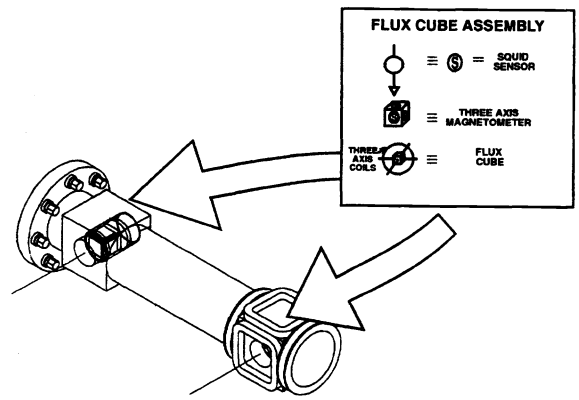

Figure 17. Concept for the laboratory prototype of a 3-channel high-T_c superconducting gradiometer utilizing the three-sensor-gradiometer concept.

CONCLUSIONS AND SUMMARY

Magnetic sensors provide one tool valuable for mobile search operations and surveys for targets with a significant magnetic signature. Superconducting SQUID-based sensors theoretically represent the most sensitive of known magnetic sensors. SQUID-based magnetometers have been demonstrated with sensitivities on the order of 1 $fT/Hz^{1/2}$ at frequencies down to 0.1 Hz, while fluxgate and total-field magnetometers are demonstrating sensitivities down to 1-10 $pT/Hz^{1/2}$ at 0.1 Hz.

The U.S. Navy has developed the Superconducting Gradiometer/Magnetometer Sensor, a superconducting gradiometer which has provided long-range detection compared to conventional, non-superconducting magnetic sensors. This sensor has been utilized to demonstrate a capability for buried mine detection and clutter rejection. As a result of the multi-channel approach, the sensor provides an accurate localization capability and multi-target discrimination. The magnetic detection-and-classification signal processing developed in conjunction with the sensor has proven to be effective, providing a fully automated, real time capability. This high-tech sensor has provided reliable, rugged performance in undersea tows conducted over a period of seven years. The sensor has been operated in the same tow vehicle adjacent to a sonar without a loss in performance. This technology is available off-the-shelf to provide the greatest capability for magnetic detection and localization ever demonstrated. Work has continued recently with this sensor under the MUDSS Project to demonstrate its utility for UXO survey.

A new approach incorporating all thin-film niobium components is being pursued for greater detection range in mobile operation. A laboratory prototype is being evaluated with white noise on the order of 50 $fT/m\text{-}Hz^{1/2}$ rising to approximately 200 $fT/m\text{-}Hz^{1/2}$ at 0.1 Hz under stationary field conditions. A field-deployable version is under development to be utilized for demonstrations of mine reconnaissance and UXO surveys.

It is only a matter of time before high-T_c devices will be available with performance comparable to that which has already been demonstrated with low-T_c devices. Magnetometer performance of 140 $fT/Hz^{1/2}$ at 1 Hz has been demonstrated under stationary field conditions. This performance is a factor over 50 times better than the performance obtained from the best commercial fluxgate magnetometers. The benefits in reduced size, longer hold times, and reduced logistics and support make the high-T_c approach attractive compared to its low-T_c counterpart.

The localization capability afforded by 5-channel gradiometers (and not previously afforded by conventional magnetic sensors) is expected to add impetus to the acceptance of magnetics for mobile applications. The development of a 5-channel fluxgate gradiometer is currently in progress. Sensitivity better than 0.3 nT/m at 0.1 Hz in motion has been demonstrated.

As a result of a much lower cost and no special support requirements, such sensors will likely be sold in larger numbers for short-range applications. Their wider usage would then enhance the opportunity to display the utility of the greater classification and localization capability afforded by the 5-channel approach. With greater acceptance of the 5-channel approach, end users will likely want to obtain sensors with greater sensitivity. It is likely that the eventual development of high-performance, reliable high-T_c gradiometers will work synergistically with an increased acceptance of the more powerful magnetic signal-processing approaches. Hopefully, the time scales for this supply and demand will be commensurate and so expedite sensor developmental efforts.

ACKNOWLEDGMENTS

This work was supported by the U.S. Office of Naval Research, the U.S. Strategic Environmental Research and Development Program, and the U.S. Small Business Innovative Research Program. Among the many individuals who supported these developments at the CSS, the author acknowledges the contributions from G.I. Allen, G. Dobeck, M.C. Froelich, J.D. Lathrop, D.J. Overway, J.W. Purpura, L. Smedley, L. Vaizer, R.F. Wiegert, and W.M. Wynn. Finally the CSS would like to acknowledge the contributions from IBM Research, Ball Aerospace, Conductus, Quantum Magnetics, Lockheed Martin Federal Systems, the Naval Research Laboratory, and the Jet Propulsion laboratory including the more recent individual efforts from R.H. Koch, J. Rozen, J.H. Eraker, J.M. Schmidt, R. Cantor, P.V. Czipott, D.K. Lathrop, D. Gambrel, and R.J. Soulen, Jr.

REFERENCES

1. T. Clem, "Nitrogen Cooled Superconducting Gradiometers for Mine Reconnaissance from Small Underwater Vehicles" in the *Proceedings of the Symposium on Autonomous Vehicles in Mine Countermeasures*, pp. 6.91-6.102, April 1995.
2. T. Clem, "Superconducting Magnetic Sensors for Mine Detection and Classification," in *Detection Technologies for Mines and Minelike Targets*,Dubey, A.C., Cindrich, I., Ralston, M. and Rigans, K., (eds.), the International Society for Optical Engineering, pp. 374-383, April 1995.
3. J.D. Lathrop, J.F. McCormick, P.J. Bernstein, J.T. Bono, D.J. Overway, G.S. Sammelmann, T.H. Chao, and K.C. Scott, "Mobile Underwater Debris Survey System (MUDSS) Feasibility Demonstration report," in *UXO Forum 1996 Conference Proceedings*, PRC Environmental Management Inc., pp. 427-436, April 1996.
4. D.C. Summey and G.J. KeKelis, "Fused airborne sensor technology," in *Detection and Remediation Technologies for Mines and Minelike Targets*, A. C. Dubey, R.L. Banard, C.J. Lowe, and J.E. McFee, Eds., the International Society for Optical Engineering, Proc. SPIE 2765, pp. 226-232, April 1996.
5. Jet Propulsion Laboratory Sensor Technology Assessment for Ordnance and Explosive Waste Detection and Location, JPL Report D-11367 Revision A, 1994.
6. W. M. Wynn, C. P. Frahm, P. J. Carroll, R. H. Clark, J. Wellhoner, and M. J. Wynn, "Advanced Superconducting Gradiometer/Magnetometer Arrays and a Novel Signal Processing Technique," IEEE Trans. on Magn., Vol. MAG-11, pp. 701-707, March 1975.
7. W.M.Wynn, Magnetic Dipole Localization using the Gradient Rate Tensor Measured by a Five-Axis Gradiometer with Known Velocity, in *Detection Technologies for Mines and Minelike Targets*, Dubey, A.C., Cindrich, I., Ralston, M. and Rigans, K., (eds.), the International Society for Optical Engineering, pp. 357-367, April1995.
8. The Jet Propulsion Laboratory, 4800 Oak Grove Dr., Pasadena, CA 91109.
9. M.G. Bello, "Hierarchial Multilayer Perceprton Network Based Fusion Algorithm for Detection/Classification of Mines using Multiple Acoustic Images and Magnetic Data," in *Detection and Remediation Technologies for Mines and Minelike Targets*, A. C. Dubey, R.L. Banard, C.J. Lowe, and J.E. McFee, Eds., the International Society for Optical Engineering, Proc. SPIE 2765, 1996, pp. 84-109, April 1996.
10. L. Smedley. and G. J. Dobeck, "Automated senor fusion for synthetic aperature sonar and magnetic gradiometer data," CSS TR-96/10, Coastal Systems Station, 1996.
11. The IBM Corp. Research Division, T. J. Watson Research Center, P.O. Box 218, Yorktown Heights, NY 10598.

12. Ball Aerospace Systems Division, P.O. Box 1062, Boulder, CO 80306-1062.

13. The Lockheed-Martin Federal Systems (formally Loral Federal Systems Company and the IBM Federal Systems Company), 9500 Godwin Drive, Manassas, VA 22110.

14. Quantum Magnetics, 7740 Kenamar Court, San Diego, CA 92121-2425.

15. Naval Research Laboratory, 4555 Overlook Ave., S.E., Washington, D.C. 20375-5000.

16. R.H. Koch, J.R. Rozen, P. Woltgens, T. Picunko, W.J. Goss, D. Gambrel, D. Lathrop, D. Overway and R.F. Wiegert, "High Performance SQUID Feedback Electronics," Rev. Sci. Instrum., vol. 67(8), pp. 2968-2976, 1996.

17. J.H. Eraker, "Sensor temperature stability performance of the Advanced Liquid Helium Dewar," in *Advances in Cryogenic Engineering*, vol. 41, in press.

18. J. Eraker, "Cryogenic nitrogen cooling systems for a deployed high temperature superconducting magnetic gradiometer system," submitted for publication in IEEE Trans. Appl. Sup., August 1996.

19. R. Cantor, L.P. Lee, M. Teepe, V. Vinetskiy, and J. Longo, "Low Noise, Single-Layer $YBa_2Cu_3O_{7-x}$ DC SQUID Magnetometers at 77K," IEEE Trans. Appl. Sup., vol. 5(2), pp. 2927-2930, 1995.

20. J.M. Schmidt, L.P. Lee, A. Mathai, A. Matlashov, M. Teepe, V. Vinetskiy, and R. Cantor, "Low-noise YBCO DC SQUID magnetometers for shielded and unshielded operation," unpublished.

21. J.W. Purpura, T.R. Clem, and R.F. Wiegert, "Nonlinear response in thin film magnetometer sense loops at 77K," IEEE Trans. Appl. Sup., vol. 5(1), pp. 3123-3126, 1995.

22. J.Z. Sun, W.J. Gallagher, and R.H. Koch, "Nonlinear hysteresis in thin film magnetometers," IEEE Trans. Appl. Sup., vol. 3(1), pp. 2022-2025, 1993.

23. J.W. Purpura and R.F. Wiegert, "Magnetic hysteresis in $YBa_2Cu_3O_{7-\delta}$ magnetometer sense loops," submitted for publication in IEEE Trans. Appl. Sup., August 1996.

24. R.H. Koch, J.Z. Sun, V. Foglietta, and W.J. Gallagher, "Flux Dam, a method to reduce extra low frequency noise when a superconducting magnetometer is exposed to a magnetic field," Appl. Phys. Lett., vol. 67(5), pp. 709-711, 1995.

25. J.W. Purpura and J.M. Schmidt, "Evaluation of a three-channel high-temperature superconducting magnetometer system," unpublished.

26. R.H.Koch, "Gradiometer having a magnetometer which cancels background magnetic field from other magnetometers," U.S. Patent No. 5,122,744, 1992.

27. R.H. Koch, J.R. Rozen, J.Z. Sun, and W.J. Gallagher, "A three sensor gradiometer," Appl. Phys. Lett., vol. 63(3), pp. 403-40 5, 1993.

28. G.I. Allen, R.H. Koch, and G. Keefe, "Unique man-portable 5 element fluxgate gradiometer system, in *Detection Technologies for Mines and Minelike Targets*, A. C. Dubey, I. Cindrich, M. Ralston, and K. Rigano, eds., the International Society for Optical Engineering, Proc. SPIE 2496, pp. 384-395, 1995.

29. R.H. Koch , G.A. Keefe, and G. Allen, "Room temperature three sensor magnetic field gradiometer," Rev. Sci. Instrum. 67(1), pp. 230-235, 1996.